Continuum Mech. Thermodyn. (2018) 30:689–708
https://doi.org/10.1007/s00161-018-0635-9

REVIEW ARTICLE

J. Nordmann · M. Aßmus · H. Altenbach

Visualising elastic anisotropy: theoretical background and computational implementation

Received: 11 December 2017 / Accepted: 31 January 2018 / Published online: 24 February 2018

Abstract In this article, we present the technical realisation for visualisations of characteristic parameters of the fourth-order elasticity tensor, which is classified by three-dimensional symmetry groups. Hereby, expressions for spatial representations of YOUNG's modulus and bulk modulus as well as plane representations of shear modulus and POISSON's ratio are derived and transferred into a comprehensible form to computer algebra systems. Additionally, we present approaches for spatial representations of both latter parameters. These three- and two-dimensional representations are implemented into the software MATrix LABoratory. Exemplary representations of characteristic materials complete the present treatise.

Keywords Linear elasticity · Anisotropy · Visualisation · MATLAB

Contents

Communicated by Andreas Öchsner.

J. Nordmann (✉) · M. Aßmus · H. Altenbach
Chair of Engineering Mechanics, Institute of Mechanics, Faculty of Mechanical Engineering, Otto von Guericke University Magdeburg, Universitätsplatz 2, 39106 Magdeburg, Germany
E-mail: joachim.nordmann@ovgu.de

1 Introduction

1.1 Motivation

In the nineteenth century, the most used material was steel. Some examples for what it was used are to build bridges, ships and engines [1]. Also, this material behaves isotropic; thus, it depends only on two material parameters and can be very good described by HOOKE's law for the design and dimensioning process. But during the twentieth century, new materials were developed which have no isotropic material behaviour, anymore. Popular representative materials which are no longer isotropic are fibre-reinforced composites [2] or single crystal alloys [3]. To describe the material behaviour of these new materials, the generalised HOOKE's law is employed. Now, in contrast to the isotropic case, 21 material parameters are required in the general anisotropic case [4–6]. Hence, it is not clear how these materials react when a load is applied and in which direction the material is strong or weak. However, these are important information in the design process, nowadays. For this purpose, we present here a possibility to visualise the four material parameters of elasticity: YOUNG's modulus, bulk modulus, shear modulus and POISSON's ratio.
At first, we give an introduction to the used notation. After this, the generalised HOOKE's law is presented and properties of the elasticity tensor are discussed. This is followed by a short introduction to symmetry groups of tensors and how many material parameters for every symmetry group are required [6–9]. Then, equations for the direction-dependent material parameters are introduced and the VOIGT scheme is presented. Further on, a modification to this notation is introduced; hence, equations in tensor and matrix notation have the same properties [10]. In the next section, the equations in tensor notation are transformed into matrix notation and afterwards an example material is visualised. Finally, brief conclusions are given.

1.2 Preliminaries and notation

Throughout the whole paper, a direct tensor notation is preferred. Only if it is conducive to the clarity of the representation and to avoid additional formal definitions, we drop this convention and use index notation instead. Zero-order tensors are symbolised by italic letters (e.g. a), first-order tensors by italic lowercase bold letters (e.g. $\boldsymbol{a} = a_i\,\boldsymbol{e}_i$ or $\boldsymbol{b} = b_j\,\boldsymbol{e}_j$), second-order tensors by italic uppercase bold letters (e.g. $\boldsymbol{A} = A_{lm}\,\boldsymbol{e}_l \otimes \boldsymbol{e}_m$ or $\boldsymbol{B} = B_{no}\,\boldsymbol{e}_n \otimes \boldsymbol{e}_o$), and fourth-order tensors by italic uppercase bold calligraphic letters (e.g. $\boldsymbol{\mathcal{A}} = A_{pqrs}\,\boldsymbol{e}_p \otimes \boldsymbol{e}_q \otimes \boldsymbol{e}_r \otimes \boldsymbol{e}_s$), where EINSTEIN summation convention is applied. Considering a CARTESian coordinate system and orthonormal bases, for example, $\{\boldsymbol{e}_i\}$, basic operations for tensors used in this paper are the scalar product

$$\boldsymbol{a} \cdot \boldsymbol{b} = a_i\,b_j\,\boldsymbol{e}_i \cdot \boldsymbol{e}_j = a_i\,b_i = \alpha \qquad \alpha \in \mathbb{R},$$

the dyadic product

$$\boldsymbol{a} \otimes \boldsymbol{b} = a_i\,b_j\,\boldsymbol{e}_i \otimes \boldsymbol{e}_j = \boldsymbol{C},$$

the composition of a second- and a first-order tensors

$$\boldsymbol{A} \cdot \boldsymbol{a} = A_{lm}\,a_i\,\boldsymbol{e}_l \otimes \boldsymbol{e}_m \cdot \boldsymbol{e}_i = A_{li}\,a_i\,\boldsymbol{e}_l = \boldsymbol{d},$$

the composition of two second-order tensors

$$\boldsymbol{A} \cdot \boldsymbol{B} = A_{lm}\,B_{no}\,\boldsymbol{e}_l \otimes \boldsymbol{e}_m \cdot \boldsymbol{e}_n \otimes \boldsymbol{e}_o = A_{lm}\,B_{mo}\,\boldsymbol{e}_l \otimes \boldsymbol{e}_o = \boldsymbol{D},$$

the double scalar product between a fourth- and a second -order tensors

$$\begin{aligned}\boldsymbol{\mathcal{A}} : \boldsymbol{B} &= A_{pqrs}\,B_{no}\,\boldsymbol{e}_p \otimes \boldsymbol{e}_q \otimes \boldsymbol{e}_r \otimes \boldsymbol{e}_s : \boldsymbol{e}_n \otimes \boldsymbol{e}_o \\ &= A_{pqrs}\,B_{sr}\,\boldsymbol{e}_p \otimes \boldsymbol{e}_q = \boldsymbol{F}\,.\end{aligned}$$

In the following equation, the KRONECKER delta δ_{ij} is used to represent the second-order unit tensor.

$$\boldsymbol{1} = \delta_{ij}\,\boldsymbol{e}_i \otimes \boldsymbol{e}_j = \boldsymbol{e}_i \otimes \boldsymbol{e}_i \quad \text{with} \quad \delta_{ij} = \begin{cases} 1 & \text{if } i = j \\ 0 & \text{if } i \neq j \end{cases}$$

Using the tensor notation, Latin indices (e.g. i, j, k, l) run through the values 1, 2 and 3, while Greek indices (e.g. $\alpha, \beta, \gamma, \delta$) run through the values 1 and 2.
In vector-matrix notation, vectors are denoted as upright lowercase sans serif bold letters (e.g. displacement vector $\mathbf{u} = [u_1\ u_2\ u_3]^\top$) and matrices as upright uppercase sans serif bold letters (e.g. elasticity matrix $\mathbf{C}$).

2 Theoretical background

2.1 Linear elasticity

In the linear elastic theory, the stress tensor $\boldsymbol{T} = T_{ij}\, \boldsymbol{e}_i \otimes \boldsymbol{e}_j$ is derived through a linear mapping of the strain tensor $\boldsymbol{E} = E_{ij}\, \boldsymbol{e}_i \otimes \boldsymbol{e}_j$ with a fourth-order tensor $\boldsymbol{\mathcal{C}} = C_{ijkl}\, \boldsymbol{e}_i \otimes \boldsymbol{e}_j \otimes \boldsymbol{e}_k \otimes \boldsymbol{e}_l$ which is called elasticity tensor. While restricting ourselves to small deformations, the resulting equation is known as generalised HOOKE's law.

$$\boldsymbol{T} = \boldsymbol{\mathcal{C}} : \boldsymbol{E} \tag{1}$$

Hereby, for $\boldsymbol{\mathcal{C}}$, following symmetries hold true [11], while $\boldsymbol{A}$ and $\boldsymbol{B}$ are selected arbitrarily:

$$\begin{aligned} \boldsymbol{A} : \boldsymbol{\mathcal{C}} : \boldsymbol{B} &= \boldsymbol{B} : \boldsymbol{\mathcal{C}} : \boldsymbol{A} & C_{ijkl} &= C_{klij} & &\text{major symmetry} \\ \boldsymbol{A} : \boldsymbol{\mathcal{C}} &= \boldsymbol{A}^{\top} : \boldsymbol{\mathcal{C}} & C_{ijkl} &= C_{jikl} & &\text{left subsymmetry} \\ \boldsymbol{\mathcal{C}} : \boldsymbol{A} &= \boldsymbol{\mathcal{C}} : \boldsymbol{A}^{\top} & C_{ijkl} &= C_{ijlk} & &\text{right subsymmetry} \end{aligned}$$

The inverse $\boldsymbol{\mathcal{S}} = \boldsymbol{\mathcal{C}}^{-1}$ is called inverse elasticity tensor while $\boldsymbol{\mathcal{S}} : \boldsymbol{\mathcal{C}} = \mathcal{I}^{\mathrm{sym}}$ holds true. Thereby, $\mathcal{I}^{\mathrm{sym}}$ stands for the symmetric fourth-order unit tensor. Furthermore, $\boldsymbol{\mathcal{C}}$ is positive definite:

$$\boldsymbol{A} : \boldsymbol{\mathcal{C}} : \boldsymbol{A} > 0 \qquad \forall\, \boldsymbol{A} \neq 0$$

Due to these properties of $\boldsymbol{\mathcal{C}}$, it is possible to determine its inverse and simply transform Eq. (1) into a vector-matrix notation. This procedure is explained in Sect. 3.

2.2 Symmetry groups

The properties of a material can depend on the loading direction or not. The latter case is called isotropic material behaviour, which is a good approximation for a lot of materials (e.g. steel, rubber). Other materials (e.g. wood, glass fibre-reinforced composites) have a dependence on the loading direction. In general, this is called anisotropic material behaviour, which is classified by 32 crystal classes [8,9]. However, eight symmetry classes $\mathbb{S}$ out of these symmetry groups are required in continuum mechanics [13]. These classes can be generated with the aid of the RAYLEIGH product [14] of an orthogonal tensor applied to the elasticity tensor. This product rotates the base of a tensor.

$$\boldsymbol{Q} \star \boldsymbol{\mathcal{C}} = C_{ijkl}\, (\boldsymbol{Q} \cdot \boldsymbol{e}_i) \otimes (\boldsymbol{Q} \cdot \boldsymbol{e}_j) \otimes (\boldsymbol{Q} \cdot \boldsymbol{e}_k) \otimes (\boldsymbol{Q} \cdot \boldsymbol{e}_l) \tag{2}$$

To derive the proper orthogonal tensor $\boldsymbol{Q}$, generators $\boldsymbol{G}$ are required. Table 1 summarises all generators for each symmetry class. Thereby, a generator describes pure rotations (no reflections) around a specific axis with a specific angle. This is denoted by a lower index and an upper index of $\boldsymbol{G}$. The lower index describes the rotation axis and upper index the angle. Moreover, Table 1 lists the number of generators (*NG*), number of planes (*NP*) and number of independent components (*NC*) for each symmetry class. Now, first generators are used to derive a new orthogonal tensor. This new tensor is combined with each generator to derive two more orthogonal tensors. They are combined again and so on. This procedure ends when no new tensor can be derived. In the last step, all derived orthogonal tensors are combined to generate $\boldsymbol{Q}$. For a better understanding, we explain this procedure for the tetragonal symmetry class, which consists of two generators and eight combination possibilities. The first step is to combine the two generators to derive the first orthogonal tensor:

$$\boldsymbol{Q}_1 = \boldsymbol{G}^{\pi}_{\boldsymbol{e}_1} \cdot \boldsymbol{G}^{3\pi/2}_{\boldsymbol{e}_3} \tag{3}$$

Up next, this new tensor is combined with the generators

$$\boldsymbol{Q}_2 = \boldsymbol{G}^{\pi}_{\boldsymbol{e}_1} \cdot \boldsymbol{Q}_1, \quad \boldsymbol{Q}_3 = \boldsymbol{G}^{3\pi/2}_{\boldsymbol{e}_3} \cdot \boldsymbol{Q}_1, \quad \text{etc.} \tag{4}$$

In this case, the procedure ends after eight different combinations because no new tensor arises. Then, the final tensor $\boldsymbol{Q}$ can be derived through combination of all $\boldsymbol{Q}_i$ with $i = \{1, \ldots, 8\}$:

$$\boldsymbol{Q} = \boldsymbol{Q}_1 \cdot \boldsymbol{Q}_2 \cdot \boldsymbol{Q}_3 \cdot \boldsymbol{Q}_4 \cdot \boldsymbol{Q}_5 \cdot \boldsymbol{Q}_6 \cdot \boldsymbol{Q}_7 \cdot \boldsymbol{Q}_8 \tag{5}$$

For more information, we refer to BERTRAM [7] or WEYL [15]. All symmetry classes have a different amount of required material parameters. In the anisotropic case, these are 21 parameters. This number is reduced for each symmetry group until only two material parameters remain in the isotropic case (see [16,17]).

Table 1 Generators according to symmetry groups of the elasticity tensor [12]

$\mathbb{S}$	$\boldsymbol{G}_k(\mathbb{S})$	$[G_{ij}]_k(\mathbb{S})$	$NG(\mathbb{S})$	$NP(\mathbb{S})$	$NC(\mathcal{C})$
Triclinic	$\mathbf{1}$	$\begin{bmatrix} 1 & 0 & 0 \\ 0 & 1 & 0 \\ 0 & 0 & 1 \end{bmatrix}$	1	0	21
Monoclinic	$\boldsymbol{G}^{\pi}_{\boldsymbol{e}_1}$	$\begin{bmatrix} 1 & 0 & 0 \\ 0 & -1 & 0 \\ 0 & 0 & -1 \end{bmatrix}$	2	1	13
Rhombic	$\boldsymbol{G}^{\pi}_{\boldsymbol{e}_1}, \boldsymbol{G}^{\pi}_{\boldsymbol{e}_2}$	$\begin{bmatrix} 1 & 0 & 0 \\ 0 & -1 & 0 \\ 0 & 0 & -1 \end{bmatrix}, \begin{bmatrix} -1 & 0 & 0 \\ 0 & 1 & 0 \\ 0 & 0 & -1 \end{bmatrix}$	4	3	9
Trigonal	$\boldsymbol{G}^{\pi}_{\boldsymbol{e}_2}, \boldsymbol{G}^{2\pi/3}_{\boldsymbol{e}_3}$	$\begin{bmatrix} -1 & 0 & 0 \\ 0 & 1 & 0 \\ 0 & 0 & -1 \end{bmatrix}, \begin{bmatrix} -1/2 & -\sqrt{3}/2 & 0 \\ -\sqrt{3}/2 & -1/2 & 0 \\ 0 & 0 & 1 \end{bmatrix}$	6	3	6
Tetragonal	$\boldsymbol{G}^{\pi}_{\boldsymbol{e}_1}, \boldsymbol{G}^{3\pi/2}_{\boldsymbol{e}_3}$	$\begin{bmatrix} 1 & 0 & 0 \\ 0 & -1 & 0 \\ 0 & 0 & -1 \end{bmatrix}, \begin{bmatrix} 0 & 1 & 0 \\ -1 & 0 & 0 \\ 0 & 0 & 1 \end{bmatrix}$	8	5	6
Hexagonal	$\boldsymbol{G}^{\pi}_{\boldsymbol{e}_1}, \boldsymbol{G}^{\pi/3}_{\boldsymbol{e}_3}$	$\begin{bmatrix} 1 & 0 & 0 \\ 0 & -1 & 0 \\ 0 & 0 & -1 \end{bmatrix}, \begin{bmatrix} 1/2 & -\sqrt{3}/2 & 0 \\ \sqrt{3}/2 & 1/2 & 0 \\ 0 & 0 & 1 \end{bmatrix}$	12	$1+\infty$	5
Cubic	$\boldsymbol{G}^{3\pi/2}_{\boldsymbol{e}_1}, \boldsymbol{G}^{2\pi/3}_{1/\sqrt{3}(\boldsymbol{e}_1+\boldsymbol{e}_2+\boldsymbol{e}_3)}$	$\begin{bmatrix} 1 & 0 & 0 \\ 0 & 0 & 1 \\ 0 & -1 & 0 \end{bmatrix}, \begin{bmatrix} 0 & 0 & 1 \\ 1 & 0 & 0 \\ 0 & 1 & 0 \end{bmatrix}$	24	9	3
Isotropic	$\boldsymbol{G}^{\psi}_{\boldsymbol{d}}$	-	∞	∞	2

2.3 Orientational dependency of characteristic parameters

A linear elastic material behaviour is described by four different parameters as long as the elasticity tensor is of rhombic or lower symmetry (e.g. cubic). Stiffness tensors of higher symmetry groups depend on two additional parameters which are called CHENCOV's and RABINOVICH's modulus [6]. The used parameters are YOUNG's modulus, bulk modulus, shear modulus and POISSON's ratio, whereby YOUNG's modulus is the most important parameter. As long as the material behaves isotropic, only two of these parameters are independent. Also, in this case, it is not necessary to visualise the parameters because only one value exists for each parameter in every direction. But when the behaviour gets anisotropic (e.g. trigonal), a dependence on the loading direction exists. It is interesting to visualise these parameters to find strongest and weakest directions, respectively.
For the sake of brevity, we renounce demonstrating the derivations of elasticity parameters with directional dependency. Thus, the explanation is shortish and performed just for YOUNG's modulus. The YOUNG's modulus is normally measured in a uni-axial tensile test in direction $\boldsymbol{d}$. This leads to following stress $\boldsymbol{T} = T\,\boldsymbol{d}\otimes\boldsymbol{d}$ and strain tensor $\boldsymbol{E} = E\,\boldsymbol{d}\otimes\boldsymbol{d}$. With the definition of YOUNG's modulus $Y = \frac{T}{E}$, it is possible to derive a final equation for the YOUNG's modulus with respect to direction $\boldsymbol{d}$:

$$Y(\boldsymbol{d}) = \left[\boldsymbol{d}\otimes\boldsymbol{d} : \boldsymbol{\mathcal{S}} : \boldsymbol{d}\otimes\boldsymbol{d}\right]^{-1} \tag{6}$$

To get a more detailed explanation and additionally an explanation for the other parameters, we refer to BÖHLKE AND BRÜGGEMANN [18], RYCHLEWSKI [19] or CURNIER [20]. In the sequel, only final equations for remaining parameters are presented since we are restricted to the application and numerical implementation of these equations to visualise elastic material parameters. Up next follows the bulk modulus

$$K(\boldsymbol{d}) = \frac{1}{3}\left[\mathbf{1} : \boldsymbol{\mathcal{S}} : \boldsymbol{d}\otimes\boldsymbol{d}\right]^{-1}, \tag{7}$$

the shear modulus

$$G(\boldsymbol{d},\boldsymbol{n}) = \frac{1}{2}\left[\frac{\sqrt{2}}{2}(\boldsymbol{d}\otimes\boldsymbol{n}+\boldsymbol{n}\otimes\boldsymbol{d}) : \boldsymbol{\mathcal{S}} : (\boldsymbol{d}\otimes\boldsymbol{n}+\boldsymbol{n}\otimes\boldsymbol{d})\frac{\sqrt{2}}{2}\right]^{-1} \tag{8}$$

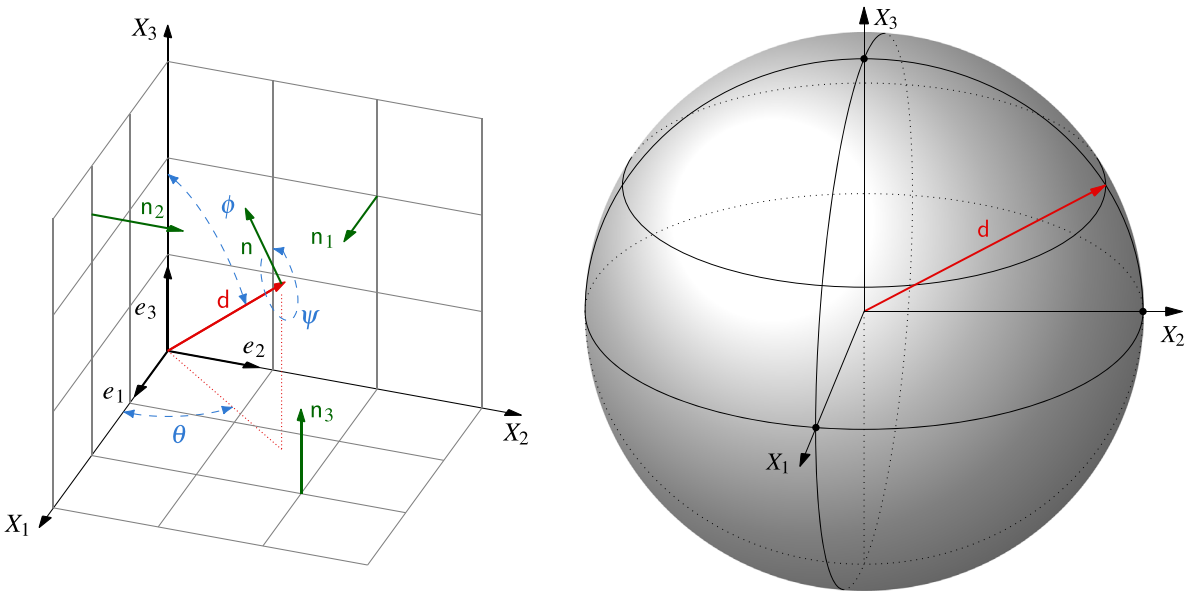

Fig. 1 Spherical coordinates and normal vectors in the EUCLIDIAN space $\mathbb{E}^3$ and resulting sphere (globular with isotropy)

and POISSON's ratio.

$$\nu\left(\boldsymbol{d},\boldsymbol{n}\right) = -Y\left(\boldsymbol{d}\right)\,\boldsymbol{d}\otimes\boldsymbol{d}:\boldsymbol{\mathcal{S}}:\boldsymbol{n}\otimes\boldsymbol{n} \tag{9}$$

For the graphical representation of material parameters, a spherical coordinate system is chosen (see Fig. 1 left) with loading direction vector $\boldsymbol{d}$, polar angles ϕ and azimuth angle θ. The length of $\boldsymbol{d}$ is equal one ($||\boldsymbol{d}|| = 1$) to ensure that the calculated material parameter is not rescaled. Additionally, for calculation of shear modulus and POISSON's ratio, a normal vector is required. Normally, therefore are only the normal vectors $\boldsymbol{n}_1$, $\boldsymbol{n}_2$ and $\boldsymbol{n}_3$ used because only shear modulus and POISSON's ratio with a loading direction vertical to these normal vectors are required for the elasticity tensor, as an example G_{12} or ν_{23}. But this would denote that it is not possible to plot these values as a solid like it is mentioned by BÖHLKE AND BRÜGGEMANN [18] or RYCHLEWSKI [19]. For this purpose, we introduce a general normal vector $\boldsymbol{n}$ vertical to $\boldsymbol{d}$ and a third angle ψ, which rotates the normal vector around the direction vector $\boldsymbol{d}$. Thus, it is possible to determine shear modulus or POISSON's ratio for every direction, respectively.

$$[d_i] = \begin{bmatrix} \sin(\phi)\cos(\theta) \\ \sin(\phi)\sin(\theta) \\ \cos(\phi) \end{bmatrix} \quad [n_i] = \begin{bmatrix} \sin(\theta)\sin(\psi) - \cos(\phi)\cos(\theta)\cos(\psi) \\ -\cos(\theta)\sin(\psi) - \cos(\phi)\sin(\theta)\cos(\psi) \\ \sin(\phi)\cos(\psi) \end{bmatrix} \quad \text{with} \quad \begin{array}{l} 0 \leqslant \phi \leqslant \pi \\ 0 \leqslant \theta \leqslant 2\pi \\ 0 \leqslant \psi \leqslant 2\pi \end{array} \tag{10}$$

This offers the possibility to visualise them as solids, too, like YOUNG's modulus and bulk modulus. However, because of rotating the normal vector $\boldsymbol{n}$ around $\boldsymbol{d}$, we have an infinite amount of solutions for every position of the direction vector. Hence, a criterion must be defined to decide which value of ψ should be plotted. Here, we investigate three different criteria. The first one is the maximum of ψ, and the second is minimum. Additionally, a third criterion is defined by an averaging scheme. We use an arithmetic average of all ψ. Other possibilities are averaging schemes after VOIGT [9], REUSS [21] or HILL [22] as examples. Of course, it is always possible to plot shear modulus and POISSON's ratio as a curve for a specific plane. What is the usual visualisation of them. Therefore, the angle ψ and a second angle (ϕ or θ) must be chosen to be constant. This depends on the plane for the material parameter (e.g. G_{12}).

The ideal shape of the solid is a sphere, which represents isotropic material behaviour. The discrepancy between solid and sphere describes the amount of anisotropy of the material. In case that shear modulus or POISSON's ratio is plotted in a plane, the ideal form is a cycle and the difference between cycle and curve represents then the amount of anisotropy.

3 Numerical implementation

3.1 Vector-matrix notation

In order to employ a computer algebra system for the computation of spatial representations of the engineering measures, it is beneficial to transfer the set of equations from tensor into a vector matrix notation. This is done by the widely used VOIGT scheme, which is based on a simple mnemonic rule. Thereby, the coefficient matrices of both tensors with respect to an orthonormal coordinate system are used. Actually, in the literature, other schemes are used too. But this results only in a permutation of shear elements in stress and strain vector and in a permutation of the corresponding rows and columns in the elasticity matrix. At first, this procedure is used to transform the stress and strain tensor. Thereby, it is important to add "2" to the strain vector; thus, the elastic energy is correctly defined.

$$[T_{ij}] = \begin{bmatrix} T_{11} & T_{12} & T_{13} \\ & T_{22} & T_{23} \\ \text{sym} & & T_{33} \end{bmatrix} \qquad [E_{ij}] = \begin{bmatrix} E_{11} & E_{12} & E_{13} \\ & E_{22} & E_{23} \\ \text{sym} & & E_{33} \end{bmatrix} \tag{11}$$

$$\mathbf{t} = \begin{bmatrix} T_{11} & T_{22} & T_{33} & T_{23} & T_{13} & T_{12} \end{bmatrix}^{\top} \quad \mathbf{e} = \begin{bmatrix} E_{11} & E_{22} & E_{33} & 2E_{23} & 2E_{13} & 2E_{12} \end{bmatrix}^{\top} \tag{12}$$

For the fourth-order elasticity tensor, the VOIGT scheme leads to a symmetric 6×6 matrix. Due to the main symmetry of $\boldsymbol{\mathcal{C}}$, this matrix is also symmetric.

$$\mathbf{C} = \begin{bmatrix} C_{1111} & C_{1122} & C_{1133} & C_{1123} & C_{1113} & C_{1112} \\ & C_{2222} & C_{2233} & C_{2223} & C_{2213} & C_{2212} \\ & & C_{3333} & C_{3323} & C_{3313} & C_{3312} \\ & & & C_{2323} & C_{2313} & C_{2312} \\ & & & & C_{1313} & C_{1312} \\ \text{sym} & & & & & C_{1212} \end{bmatrix} \tag{13}$$

The generalised HOOKE's law can thus also be written in vector-matrix form

$$\mathbf{t} = \mathbf{C}\,\mathbf{e} \quad \text{or equivalently} \quad \begin{bmatrix} T_{11} \\ T_{22} \\ T_{33} \\ T_{23} \\ T_{13} \\ T_{12} \end{bmatrix} = \begin{bmatrix} C_{1111} & C_{1122} & C_{1133} & C_{1123} & C_{1113} & C_{1112} \\ & C_{2222} & C_{2233} & C_{2223} & C_{2213} & C_{2212} \\ & & C_{3333} & C_{3323} & C_{3313} & C_{3312} \\ & & & C_{2323} & C_{2313} & C_{2312} \\ & & & & C_{1313} & C_{1312} \\ \text{sym} & & & & & C_{1212} \end{bmatrix} \begin{bmatrix} E_{11} \\ E_{22} \\ E_{33} \\ 2E_{23} \\ 2E_{13} \\ 2E_{12} \end{bmatrix}. \tag{14}$$

This form is widespread. It is found in most of the textbooks on solid mechanics and is used in almost all commercial finite element program systems. But problems arise when considering anisotropies with this representation because it is inconsistent due to following issues.

$$\mathbf{t}^{\top}\mathbf{t} \neq \boldsymbol{T} : \boldsymbol{T} \qquad \mathbf{e}^{\top}\mathbf{e} \neq \boldsymbol{E} : \boldsymbol{E} \qquad \text{but } \mathbf{t}^{\top}\mathbf{e} = \boldsymbol{T} : \boldsymbol{E}$$

Hence, invariants, eigenvalues and eigentensors of $\boldsymbol{\mathcal{C}}$ cannot be determined by means of the square matrix $\mathbf{C}$. To overcome this shortcomings, FEDOROV [10] derived an alternative form to represent the elasticity tensor by a 6×6 matrix, see also [23].

$$\begin{bmatrix} T_{11} \\ T_{22} \\ T_{33} \\ \sqrt{2}T_{23} \\ \sqrt{2}T_{13} \\ \sqrt{2}T_{12} \end{bmatrix} = \begin{bmatrix} C_{1111} & C_{1122} & C_{1133} & \sqrt{2}C_{1123} & \sqrt{2}C_{1113} & \sqrt{2}C_{1112} \\ & C_{2222} & C_{2233} & \sqrt{2}C_{2223} & \sqrt{2}C_{2213} & \sqrt{2}C_{2212} \\ & & C_{3333} & \sqrt{2}C_{3323} & \sqrt{2}C_{3313} & \sqrt{2}C_{3312} \\ & & & 2C_{2323} & 2C_{2313} & 2C_{2312} \\ & & & & 2C_{1313} & 2C_{1312} \\ \text{sym} & & & & & 2C_{1212} \end{bmatrix} \begin{bmatrix} E_{11} \\ E_{22} \\ E_{33} \\ 2\sqrt{2}E_{23} \\ 2\sqrt{2}E_{13} \\ 2\sqrt{2}E_{12} \end{bmatrix} \tag{15}$$

Because of the previously mentioned facts, we use FEDOROV form of generalised HOOKE's law in this work, which is mathematically consistent, additionally. This normalised form of the VOIGT notation is also known as MANDEL notation [24]. Others [23] coined the term KELVIN notation to honour the inventor of this notation, Lord KELVIN [25].

3.2 Elasticity matrices

With the aid of the vector-matrix notation, it is trivial to represent the elasticity matrices resulting from Sect. 2.2, see [26]. In the sequel, we list eight different elasticity matrices according to the symmetry groups introduced in Sect. 2.2. We also give the number of independent constants *NC* and the number of symmetry planes *NP* of each group, as stated in [18]. See also Table 1.

triclinic ($NC = 21$, $NP = 0$)

$$\mathbf{C} = \begin{bmatrix} C_{1111} & C_{1122} & C_{1133} & \sqrt{2}C_{1123} & \sqrt{2}C_{1113} & \sqrt{2}C_{1112} \\ & C_{2222} & C_{2233} & \sqrt{2}C_{2223} & \sqrt{2}C_{2213} & \sqrt{2}C_{2212} \\ & & C_{3333} & \sqrt{2}C_{3323} & \sqrt{2}C_{3313} & \sqrt{2}C_{3312} \\ & & & 2C_{2323} & 2C_{2313} & 2C_{2312} \\ & & & & 2C_{1313} & 2C_{1312} \\ \text{sym} & & & & & 2C_{1212} \end{bmatrix} \tag{16}$$

monoclinic ($NC = 13$, $NP = 1$)

$$\mathbf{C} = \begin{bmatrix} C_{1111} & C_{1122} & C_{1133} & \sqrt{2}C_{1123} & 0 & 0 \\ & C_{2222} & C_{2233} & \sqrt{2}C_{2223} & 0 & 0 \\ & & C_{3333} & \sqrt{2}C_{3323} & 0 & 0 \\ & & & 2C_{2323} & 0 & 0 \\ & & & & 2C_{1313} & 2C_{1312} \\ \text{sym} & & & & & 2C_{1212} \end{bmatrix} \tag{17}$$

rhombic ($NC = 9$, $NP = 3$)

$$\mathbf{C} = \begin{bmatrix} C_{1111} & C_{1122} & C_{1133} & 0 & 0 & 0 \\ & C_{2222} & C_{2233} & 0 & 0 & 0 \\ & & C_{3333} & 0 & 0 & 0 \\ & & & 2C_{2323} & 0 & 0 \\ & & & & 2C_{1313} & 0 \\ \text{sym} & & & & & 2C_{1212} \end{bmatrix} \tag{18}$$

trigonal ($NC = 6$, $NP = 3$)

$$\mathbf{C} = \begin{bmatrix} C_{1111} & C_{1122} & C_{1133} & \sqrt{2}C_{1123} & 0 & 0 \\ & C_{2222} & C_{1133} & -\sqrt{2}C_{1123} & 0 & 0 \\ & & C_{3333} & 0 & 0 & 0 \\ & & & 2C_{2323} & 0 & 0 \\ & & & & 2C_{2323} & 2C_{1123} \\ \text{sym} & & & & & C_{1111} - C_{1122} \end{bmatrix} \tag{19}$$

tetragonal ($NC = 6$, $NP = 5$)

$$\mathbf{C} = \begin{bmatrix} C_{1111} & C_{1122} & C_{1133} & 0 & 0 & 0 \\ & C_{2222} & C_{1133} & 0 & 0 & 0 \\ & & C_{3333} & 0 & 0 & 0 \\ & & & 2C_{2323} & 0 & 0 \\ & & & & 2C_{2323} & 0 \\ \text{sym} & & & & & 2C_{1212} \end{bmatrix} \tag{20}$$

hexagonal ($NC = 5$, $NP = 1 + \infty$)

$$\mathbf{C} = \begin{bmatrix} C_{1111} & C_{1122} & C_{1133} & 0 & 0 & 0 \\ & C_{1111} & C_{1133} & 0 & 0 & 0 \\ & & C_{3333} & 0 & 0 & 0 \\ & & & 2C_{2323} & 0 & 0 \\ & & & & 2C_{2323} & 0 \\ \text{sym} & & & & & C_{1111} - C_{1122} \end{bmatrix} \tag{21}$$

cubic ($NC = 3$, $NP = 9$)

$$\mathbf{C} = \begin{bmatrix} C_{1111} & C_{1122} & C_{1122} & 0 & 0 & 0 \\ & C_{1111} & C_{1122} & 0 & 0 & 0 \\ & & C_{1111} & 0 & 0 & 0 \\ & & & 2C_{2323} & 0 & 0 \\ & & & & 2C_{2323} & 0 \\ \text{sym} & & & & & 2C_{2323} \end{bmatrix} \tag{22}$$

isotropic ($NC = 2$, $NP = \infty$)

$$\mathbf{C} = \begin{bmatrix} C_{1111} & C_{1122} & C_{1122} & 0 & 0 & 0 \\ & C_{1111} & C_{1122} & 0 & 0 & 0 \\ & & C_{1111} & 0 & 0 & 0 \\ & & & 2\,(C_{1111} - C_{1122}) & 0 & 0 \\ & & & & 2\,(C_{1111} - C_{1122}) & 0 \\ \text{sym} & & & & & 2\,(C_{1111} - C_{1122}) \end{bmatrix} \tag{23}$$

3.3 Implementation

Up next, we transform all other tensors of Eqs. (6), (7), (8) and (9) with the VOIGT scheme. The resulting vectors are marked with "V". Thereby, a $\sqrt{2}$ term is added to the VOIGT vectors. This is important to guarantee that properties of the vector are same as the ones of the tensor (see Sect. 3).

$$\boldsymbol{D} = \boldsymbol{d} \otimes \boldsymbol{d} = \begin{bmatrix} d_1d_1 & d_1d_2 & d_1d_3 \\ & d_2d_2 & d_2d_3 \\ \text{sym} & & d_3d_3 \end{bmatrix} \boldsymbol{e}_i \otimes \boldsymbol{e}_j \quad \Longleftrightarrow \quad \mathbf{d}_\mathrm{V} = \begin{bmatrix} d_1d_1 \\ d_2d_2 \\ d_3d_3 \\ \sqrt{2}d_2d_3 \\ \sqrt{2}d_1d_3 \\ \sqrt{2}d_1d_2 \end{bmatrix} \tag{24}$$

$$\boldsymbol{N} = \boldsymbol{n} \otimes \boldsymbol{n} = \begin{bmatrix} n_1n_1 & n_1n_2 & n_1n_3 \\ & n_2n_2 & n_2n_3 \\ \text{sym} & & n_3n_3 \end{bmatrix} \boldsymbol{e}_i \otimes \boldsymbol{e}_j \quad \Longleftrightarrow \quad \mathbf{n}_\mathrm{V} = \begin{bmatrix} n_1n_1 \\ n_2n_2 \\ n_3n_3 \\ \sqrt{2}n_2n_3 \\ \sqrt{2}n_1n_3 \\ \sqrt{2}n_1n_2 \end{bmatrix} \tag{25}$$

$$\boldsymbol{M} = \frac{\sqrt{2}}{2}\,(\boldsymbol{d} \otimes \boldsymbol{n} + \boldsymbol{n} \otimes \boldsymbol{d}) = \frac{\sqrt{2}}{2} \begin{bmatrix} d_1n_1 + n_1d_1 & d_1n_2 + n_1d_2 & d_1n_3 + n_1d_3 \\ & d_2n_2 + n_2d_2 & d_2n_3 + n_2d_3 \\ \text{sym} & & d_3n_3 + n_3d_3 \end{bmatrix} \boldsymbol{e}_i \otimes \boldsymbol{e}_j$$

$$\Longleftrightarrow \quad \mathbf{m}_\mathrm{V} = \frac{\sqrt{2}}{2} \begin{bmatrix} 2d_1n_1 \\ 2d_2n_2 \\ 2d_3n_3 \\ \sqrt{2}\,(d_2n_3 + n_2d_3) \\ \sqrt{2}\,(d_1n_3 + n_1d_3) \\ \sqrt{2}\,(d_1n_2 + n_1d_2) \end{bmatrix} \tag{26}$$

$$\mathbf{1} = \delta_{ij}\boldsymbol{e}_i \otimes \boldsymbol{e}_j = \begin{bmatrix} 1 & 0 & 0 \\ & 1 & 0 \\ \text{sym} & & 1 \end{bmatrix} \boldsymbol{e}_i \otimes \boldsymbol{e}_j \quad \Longleftrightarrow \quad \mathbf{1}_\mathrm{V} = \begin{bmatrix} 1 \\ 1 \\ 1 \\ 0 \\ 0 \\ 0 \end{bmatrix} \tag{27}$$

With these vectors, Eqs. (6), (7), (8) and (9) of the foregoing section are rewritten. The final equations are:

$$Y(\mathbf{d}) = \left[\mathbf{d}_\mathrm{V}^\top \mathbf{S}\, \mathbf{d}_\mathrm{V}\right]^{-1} \tag{28}$$

$$K(\mathbf{d}) = \left[3\, \mathbf{1}_\mathrm{V}^\top \mathbf{S}\, \mathbf{d}_\mathrm{V}\right]^{-1} \tag{29}$$

$$G(\mathbf{d}, \mathbf{n}) = \left[2\, \mathbf{m}_\mathrm{V}^\top \mathbf{S}\, \mathbf{m}_\mathrm{V}\right]^{-1} \tag{30}$$

$$\nu(\mathbf{d}, \mathbf{n}) = -Y(\mathbf{d})\, \mathbf{d}_\mathrm{V}^\top \mathbf{S}\, \mathbf{n}_\mathrm{V} \tag{31}$$

Therein, the inverse elasticity matrix $\mathbf{S}$ is derived in the same way as the inverse elasticity tensor $\mathcal{S}$ ($\mathbf{S} = \mathbf{C}^{-1}$). In MATLAB, this is performed by a LU decomposition. For further information, we refer to the specific literature, for example, [27]. Now, it is possible to do calculations with these equations and visualise the elastic properties of a material.

4 Application

In this section, we explain the application of Eqs. (28), (29), (30) and (31) to visualise elastic material properties, and as an example, we use silicon which has a cubic symmetry and the following elasticity matrix. It must be remarked that values of the lower 3×3 matrix have to be multiplied by "2", according to Eq. (22).

$$\mathbf{C} = \begin{bmatrix} 165.7 & 63.9 & 63.9 & 0 & 0 & 0 \\ & 165.7 & 63.9 & 0 & 0 & 0 \\ & & 165.7 & 0 & 0 & 0 \\ & & & 79.6 & 0 & 0 \\ & & & & 79.6 & 0 \\ \text{sym.} & & & & & 79.6 \end{bmatrix} \text{GPa}$$

Figure 2 presents the results of Eq. (28). At top, the spherical plot of the YOUNG's modulus shows that silicon has a great amount of anisotropy. Further on, it shows that in axis direction, silicon has the smallest values of YOUNG's modulus and in transverse directions the greatest values. This is also confirmed by the polar plots at the bottom of Fig. 2. Up next, the compression modulus is presented in Fig. 3. The spherical plot shows that this material parameter is isotropic, which is confirmed by the polar plots, additionally. After these easy interpretations, we explain the visualisation of shear modulus, which is shown in Fig. 4. In Eqs. (30) and (31) can be seen that shear modulus and POISSON's ratio depend on the direction vector $\mathbf{d}$ and the normal vector $\mathbf{n}$. This purpose induced that not only one shear modulus or POISSON's ratio for every direction $\mathbf{d}$ can be determined. Like it was mentioned before, an infinite amount of solutions exists because the normal vector rotates around the direction vector. To overcome this problem, we use the before-mentioned criteria. Maximum and minimum criterion is clear. For averaging, an arithmetic scheme is chosen.

$$\bar{x} = \frac{x_1 + \cdots + x_\mathrm{n}}{n} \quad n \in \mathbb{N}$$

The results of this process are presented in Figs. 4 and 5 at top. The picture at top-left position shows the maximum criterion, top-right presents the minimum criterion and in top-centre position, the average criterion is presented. At the bottom of Figs. 4 and 5, polar plots for the three main planes of a coordinate system are presented. This is done to present the common visualisation of these two material parameters. Like it was mentioned by BÖHLKE AND BRÜGGEMANN [18] or RYCHLEWSKI [19], a visualisation of shear modulus and POISSON's ratio as solid is not possible and not needed since for the elasticity or inverse elasticity tensor, only shear modulus and POISSON's ratio related to a specific plane are required (e.g. G_{12}, ν_{23}). The visualisation as a solid is only possible because of the mathematical trick by introducing the normal vector which rotates around the direction vector. What leads to the consequence that an infinite amount of solution exists which is why a criterion must be defined.

By comparing the polar plots with the spherical plots, it can be seen that the polar plots are inside the spherical plot for the maximum criterion. For the other two criteria, different solids occur and the curves cannot be found in them. Thus, we conclude that spherical visualisation of shear modulus and POISSON's ratio is possible if the correct criterion is defined. But further investigations with the maximum criterion showed that it is only

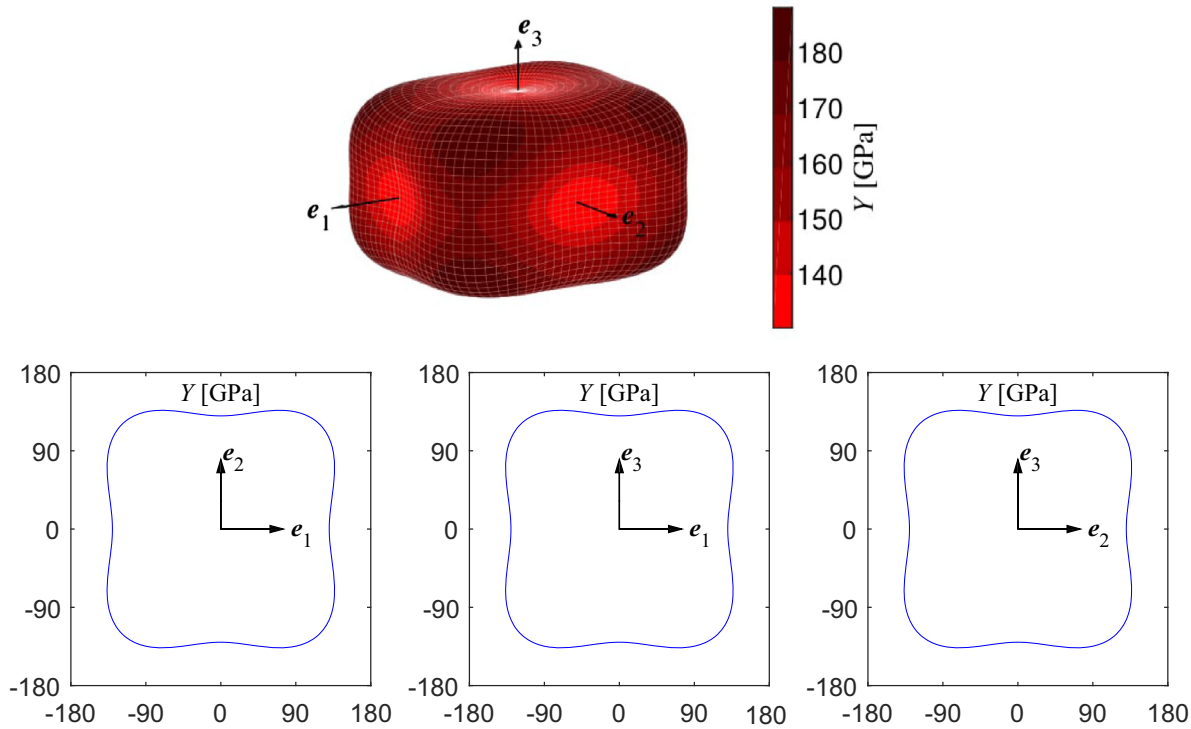

Fig. 2 Visualisation of YOUNG's modulus: spherical plot (top) and polar plots of the three main planes $\boldsymbol{e}_1 - \boldsymbol{e}_2$ (bottom, left), $\boldsymbol{e}_1 - \boldsymbol{e}_3$ (bottom, centre) and $\boldsymbol{e}_2 - \boldsymbol{e}_3$ (bottom, right) of EUCLIDIAN space $\mathbb{E}^3$

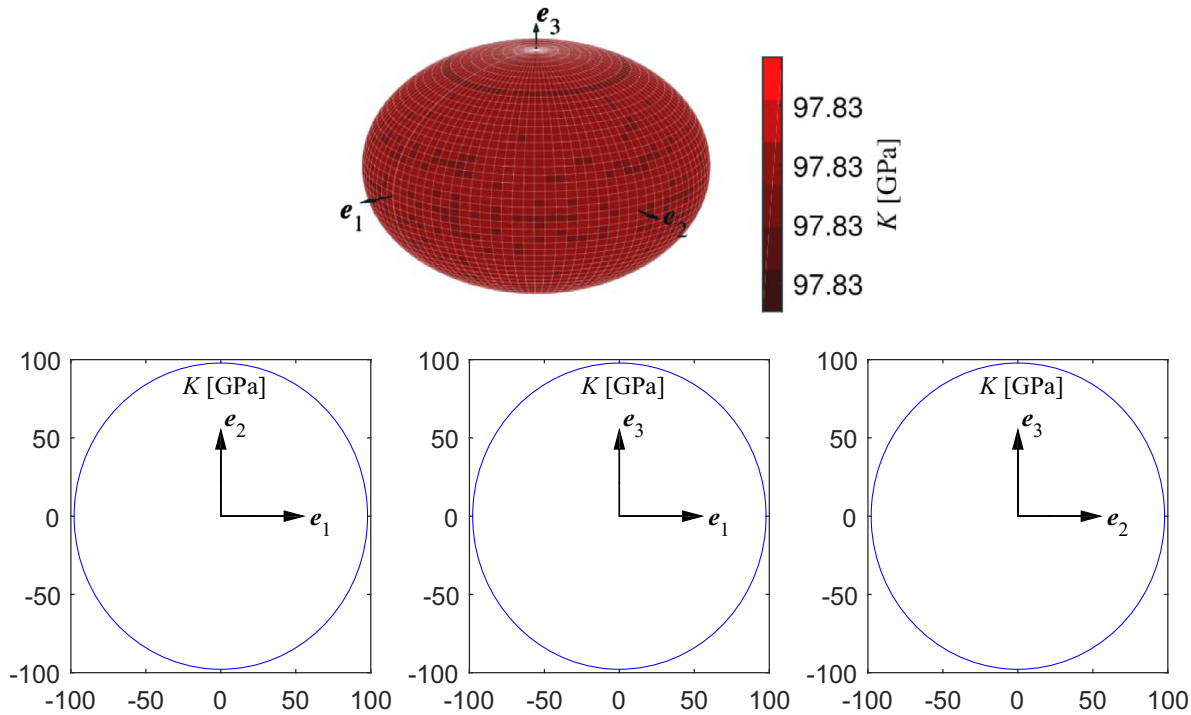

Fig. 3 Visualisation of compression modulus: spherical plot (top) and polar plots of the three main planes $\boldsymbol{e}_1 - \boldsymbol{e}_2$ (bottom, left), $\boldsymbol{e}_1 - \boldsymbol{e}_3$ (bottom, centre) and $\boldsymbol{e}_2 - \boldsymbol{e}_3$ (bottom, right) of EUCLIDIAN space $\mathbb{E}^3$

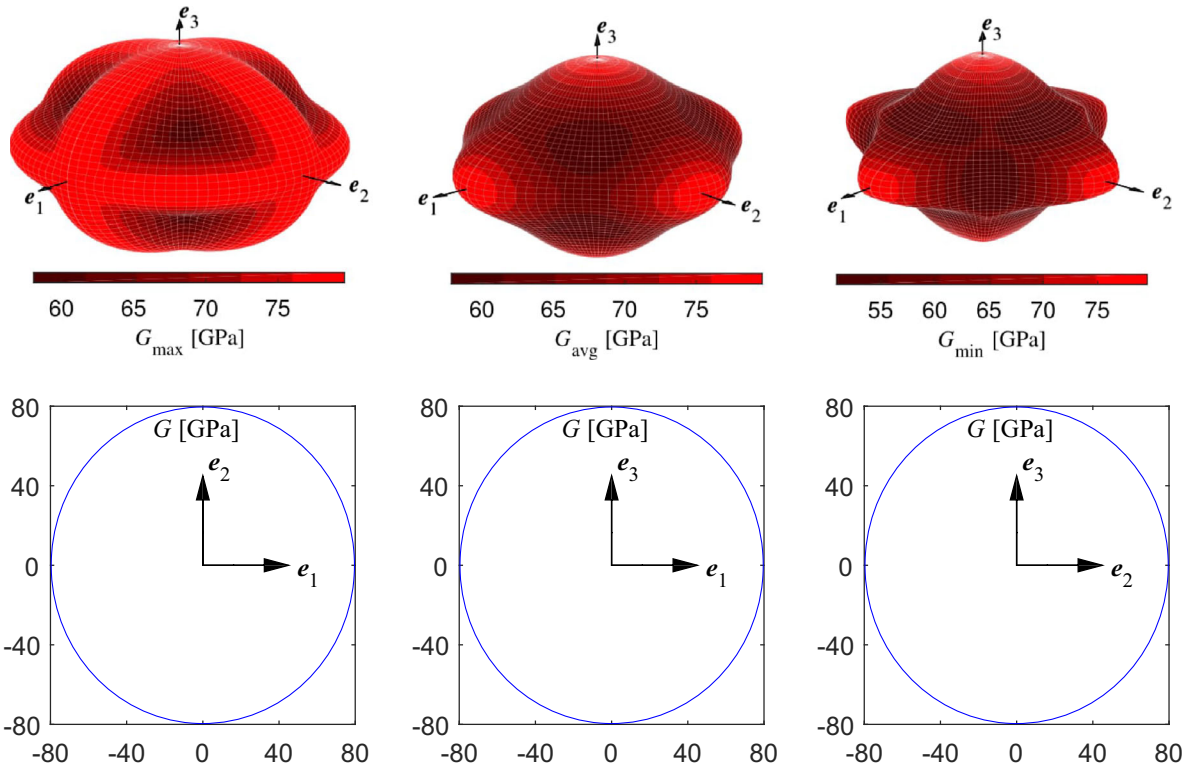

Fig. 4 Visualisation of shear modulus: spherical plots with maximum (top, left), average (top, centre) and minimum criterion (top, right) and polar plots of the three main planes $\boldsymbol{e}_1 - \boldsymbol{e}_2$ (bottom, left), $\boldsymbol{e}_1 - \boldsymbol{e}_3$ (bottom, centre) and $\boldsymbol{e}_2 - \boldsymbol{e}_3$ (bottom, right) of EUCLIDIAN space $\mathbb{E}^3$

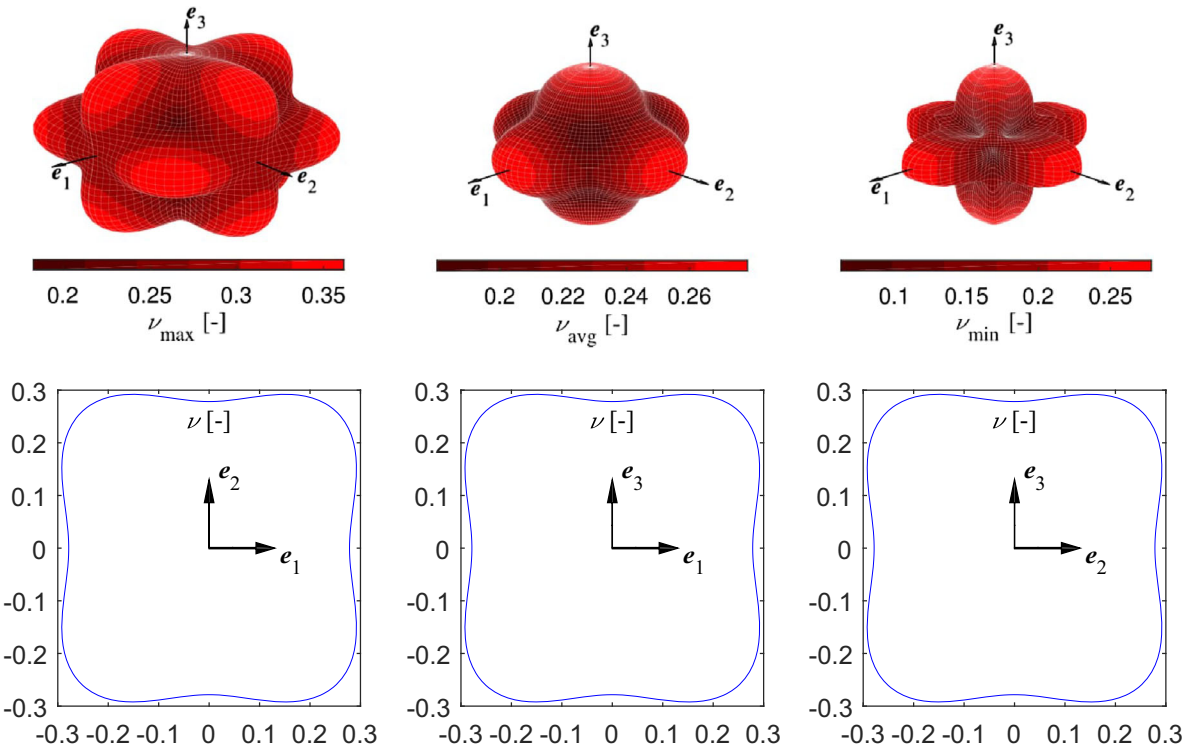

Fig. 5 Visualisation of POISSON's ratio: spherical plots with maximum (top, left), average (top, centre) and minimum criterion (top, right) and polar plots of the three main planes $\boldsymbol{e}_1 - \boldsymbol{e}_2$ (bottom, left), $\boldsymbol{e}_1 - \boldsymbol{e}_3$ (bottom, centre) and $\boldsymbol{e}_2 - \boldsymbol{e}_3$ (bottom, right) of EUCLIDIAN space $\mathbb{E}^3$

capable to visualise the isotropic and cubic symmetry group. Whereby, one restriction exits for the correct working of the maximum criterion. The minor matrix elements of elasticity, respectively, inverse elasticity matrix must be nonnegative. Otherwise, the calculated solid does not contain polar plots. This discovery is the basis for following hypothesis:
"It exists a criterion for every symmetry group of elasticity or inverse elasticity tensor, thus, that shear modulus and POISSON's ratio can be correct visualised as a solid".

5 Conclusion

In the foregoing investigations, we have presented the theory of symmetry groups and how it is possible to visualise the elastic material parameters YOUNG's modulus, bulk modulus, shear modulus and POISSON's ratio. Further on, we explained a possibility to plot shear modulus and POISSON's ratio in a spherical plot, like YOUNG's modulus and bulk modulus. Therefore, we introduced everything in tensor notation and performed then the transformation of these equations with VOIGT notation. At the end, silicon as an example material is visualised. By analysing the plots, it is investigated that the maximum criterion is capable of generating correct spherical plots of shear modulus and POISSON's ratio. Thus, the statement that shear modulus and POISSON's ratio cannot be visualised by a spherical plot [18,19] is disproved for isotropic and cubic symmetry group.
In future, it should be investigated if other criteria exist such that it gets possible to visualise shear modulus and POISSON's ratio of other symmetry groups (e.g. rhombic) and a step size control for the angles should be added to investigate elasticity matrices with a high difference in the matrix elements efficiently.
Besides our algorithm, two more exist, which are called ElAM [28] and ELATE [29], and both are open-source algorithms, too. All these algorithms perform similar calculations and create three-dimensional solids of the four material parameters YOUNG's modulus, bulk modulus, shear modulus and POISSON's ratio. However, in the present paper, the complete theory, how these algorithms are derived, is explained in detail and we make no use of averaging schemes according to VOIGT, REUSS or HILL. Further on, we do not perform an eigenvalue analysis since there is no need. The positive semi-definiteness of the elastic strain energy induces the positive definiteness of the elasticity tensor. The last benefit of this algorithm is it is developed within the software MATLAB, which is widely used in engineering science. Hence, everybody can use and manipulate the source code easily regarding his concerns. One concern could be to create three-dimensional solids of the two additional material parameters, which exist when monoclinic or triclinic symmetry classes are investigated [6]. Another possible interest could be to visualise the sixth-order elasticity tensor arising in gradient elasticity [30,31]. The transformation of this tensor results in a 18×18 matrix with 171 independent components in general anisotropic case and 5 independent components for the isotropic case [31]. At first, the isotropic case should be investigated, and as a result, every material parameter should yield a sphere. But the problem is that test definitions must be defined, and for this purpose, the meaning of the material parameters of sixth-order elasticity tensor must be clarified. Additionally, it must be clarified how the third-order stress and strain tensors look like and how the elements of these tensors are connected to the 5 independent material parameters of sixth-order elasticity tensor. When this is done, a visualisation is possible but the computational effort is much higher because the sixth-order elasticity tensor contains nine times more elements as the fourth-order elasticity tensor. Needless to say, if only a visualisation of the parameters under a mathematical motivation is required, random tests can be defined but this is out of scope for engineering science.

Acknowledgements The financial support rendered by the German Research Foundation (DFG) in context of the research training group "Micro–Macro-Interactions in Structured Media and Particle Systems" (RTG 1554) is gratefully acknowledged. The authors are thankful to Otto T. Bruhns for the clarification of the Rayleigh product's origin and to Rainer Glüge for the informative discussion about gradient elasticity and sixth-order elasticity tensors.

A Appendix

A.1 Deriving formulation of the normal vector

The normal vector $\boldsymbol{n}$ has the following properties

$$||\boldsymbol{n}|| = 1 \quad \boldsymbol{d} \cdot \boldsymbol{n} = 0 \tag{A.1}$$

and is defined as

$$\boldsymbol{n} = \begin{bmatrix} \sin\left(\phi - \frac{\pi}{2}\right)\cos(\theta) \\ \sin\left(\phi - \frac{\pi}{2}\right)\sin(\theta) \\ \cos\left(\phi - \frac{\pi}{2}\right) \end{bmatrix} \boldsymbol{e}_i . \tag{A.2}$$

With this definition the vector is orthogonal to the vector $\boldsymbol{d}$ but do not rotate around this vector. Up next, an orthogonal tensor is defined who rotates the normal vector $\boldsymbol{n}$ around the direction vector $\boldsymbol{d}$.

$$\boldsymbol{Q}(\boldsymbol{d}, \psi) = \boldsymbol{d} \otimes \boldsymbol{d} + \cos(\psi)(\mathbf{1} - \boldsymbol{d} \otimes \boldsymbol{d}) + \sin(\psi)(\boldsymbol{d} \times \mathbf{1}) \tag{A.3}$$

And with the scalar product between $\boldsymbol{Q}$ and $\boldsymbol{n}$ the final formulation for the normal vector is derived, with the ability to rotate around the direction vector $\boldsymbol{d}$ and be in every point orthogonal to this vector.

$$\boldsymbol{n} = \boldsymbol{Q} \cdot \boldsymbol{n} = \begin{bmatrix} \sin(\theta)\sin(\psi) - \cos(\phi)\cos(\theta)\cos(\psi) \\ -\cos(\theta)\sin(\psi) - \cos(\phi)\sin(\theta)\cos(\psi) \\ \sin(\phi)\cos(\psi) \end{bmatrix} \boldsymbol{e}_i \tag{A.4}$$

A.2 MATLAB source code

```
clear all;
clc;
%% Input
% As input only the stiffness matrix in the correct Voigt Notation and the
% division of azimuth angle are required. At the end this code produces 4
% plots for the different material parameters.
% The azimuth angle is in the range of 0 to 2*pi, the elongation angle goes
% from 0 to pi and the rotation angle psi is in the range of 0 to 2* pi too.
%
% Scheme for the stiffness matrix
%
% C = [          C11          C12          C13 sqrt(2)*C14 sqrt(2)*C15 sqrt(2)*C16;
%                C12          C22          C23 sqrt(2)*C24 sqrt(2)*C25 sqrt(2)*C26;
%                C13          C23          C33 sqrt(2)*C34 sqrt(2)*C35 sqrt(2)*C36;
%       sqrt(2)*C14 sqrt(2)*C24 sqrt(2)*C34        2*C44        2*C45        2*C46;
%       sqrt(2)*C15 sqrt(2)*C25 sqrt(2)*C35        2*C45        2*C55        2*C56;
%       sqrt(2)*C16 sqrt(2)*C26 sqrt(2)*C36        2*C46        2*C56        2*C66 ];


% Division / Elements of the azimuth angle
n          = 70;
% Division / Elements of the elongation angle
m          = n/2;
% Division / Elements of the rotation angle
o          = 360;
% Silicon in GPa (Values are from [18])
C      = [ 165.7  63.9  63.9  0     0     0;
            63.9 165.7  63.9  0     0     0;
            63.9  63.9 165.7  0     0     0;
             0     0     0   2*79.6  0     0;
             0     0     0     0   2*79.6  0;
             0     0     0     0     0   2*79.6 ];

% Test materials in Voigt-Notation
```

```
% EVA+Si in GPa (Values are from [32])
% C = [ 495.29  18.2  13.2  0    0         0;
%        18.2  495.29 13.2  0    0         0;
%        13.2   13.2  22.68 0    0         0;
%         0      0     0    2*3.46 0        0;
%         0      0     0    0    2*3.46     0;
%         0      0     0    0    0    2*40000 ]/1000;

% Cooper in GPa (Values are from [18])
% C     = [ 168   121.4 121.4    0       0       0;
%           121.4 168   121.4    0       0       0;
%           121.4 121.4 168      0       0       0;
%             0     0     0    2*75.4    0       0;
%             0     0     0       0    2*75.4    0;
%             0     0     0       0       0    2*75.4 ];

% Gold in GPa (Values are from [18])
% C     = [ 185 158 158  0    0    0;
%           158 185 158  0    0    0;
%           158 158 185  0    0    0;
%             0   0   0 2*39.7  0    0;
%             0   0   0  0   2*39.7  0;
%             0   0   0  0    0   2*39.7 ];

% Magnesium in GPa (Values are from [18])
% C     = [ 56.49 23.16 18.10    0       0         0;
%           23.16 56.49 18.10    0       0         0;
%           18.10 18.10 58.73    0       0         0;
%             0     0     0    2*16.81    0        0;
%             0     0     0       0    2*16.81     0;
%             0     0     0       0       0    (56.49-23.16) ];

% Feldspar in GPa (Values are from [18])
% C     = [ 61.9  43.4  36.8 -sqrt(2)*10       0         0;
%           43.4 158.3  21.8 -sqrt(2)* 1.8     0         0;
%           36.8  21.8 100.2 -sqrt(2)*12.1     0         0;
%            0     0   -sqrt(2)*12.1  2*14.1   0         0;
%            0     0   -sqrt(2)* 1.8   0    2*20.3   -2* 2.3;
%            0     0   -sqrt(2)*10     0   -2* 2.3    2*36 ];

% Pyrite in GPa (Values are from [18])
% C     = [ 361.88 -47.96 -47.96     0         0         0;
%           -47.96 361.88 -47.96     0         0         0;
%           -47.96 -47.96 361.88     0         0         0;
%             0   0  0            2*105.49     0         0;
%             0   0  0               0    2*105.49     0;
%             0   0  0               0         0    2*105.49 ];

% Weissblech in GPa (Values are from [18])
% C     = [ 76.19 71.10  67.68     0     0     0;
%           71.10 76.19  67.68     0     0     0;
%           67.68 67.68 116.24     0     0     0;
%            0     0     0     2*17.04  0     0;
%            0     0     0      0    2*17.04  0;
%            0     0     0      0     0    2*19.8 ];

% Isotropic testmaterial. Deriving the compliance matrix in line 151
  must
% be deactivated by using this material.
% Material parameters are defined randomly. Just for debugging.
  Solutions
% are spheres with a radius of Y or nue.
% Y = 100000;
% nue = 0.25;
% S = [   1/Y, -nue/Y, -nue/Y,    0,           0,           0;
%      -nue/Y,    1/Y, -nue/Y,    0,           0,           0;
%      -nue/Y, -nue/Y,    1/Y,    0,           0,           0;
%         0,      0,      0,   2*(1+nue)/Y/2,    0,           0;
%         0,      0,      0,      0,         2*(1+nue)/Y/2,    0;
```

```
%          0,      0,      0,      0,            0,          2*(1+nue)/Y
    /2];

%% Definition of the Memory
% Angles
phi         = linspace(0,  pi,m);
theta       = linspace(0,2*pi,n);
psi         = linspace(0,2*pi,o);
% Young's modulus
E           = zeros(m,n);
% Bulk modulus
K           = zeros(m,n);
% Normal vector
nn          = zeros(3,o);
% Poisson ratio
nu          = zeros(1,o);
nu_max      = zeros(m,n);
nu_min      = zeros(m,n);
nu_avg      = zeros(m,n);
% Shear modulus
G           = zeros(1,o);
G_max       = zeros(m,n);
G_min       = zeros(m,n);
G_avg       = zeros(m,n);
% Vectors for the cartesian coordinates
x_E         = zeros(m,n);
y_E         = zeros(m,n);
z_E         = zeros(m,n);
x_K         = zeros(m,n);
y_K         = zeros(m,n);
z_K         = zeros(m,n);
x_nu_max    = zeros(m,n);
y_nu_max    = zeros(m,n);
z_nu_max    = zeros(m,n);
x_nu_min    = zeros(m,n);
y_nu_min    = zeros(m,n);
z_nu_min    = zeros(m,n);
x_nu_avg    = zeros(m,n);
y_nu_avg    = zeros(m,n);
z_nu_avg    = zeros(m,n);
x_G_max     = zeros(m,n);
y_G_max     = zeros(m,n);
z_G_max     = zeros(m,n);
x_G_min     = zeros(m,n);
y_G_min     = zeros(m,n);
z_G_min     = zeros(m,n);
x_G_avg     = zeros(m,n);
y_G_avg     = zeros(m,n);
z_G_avg     = zeros(m,n);
% Calculation of the compliance matrix
S      = C^-1;
%% Calculation of Young's and bulk modulus
% Definition of the unit tensor in Voigt-notation
U_V    = [ 1;
           1;
           1;
           0;
           0;
           0 ];
for i = 1:1:n
    for j = 1:1:m
    % Direction vector with radius r=1
    d       = [ sin(phi(1,j))*cos(theta(1,i));
                sin(phi(1,j))*sin(theta(1,i));
                cos(phi(1,j)) ];
    % Calculation of the tensor D, d dyadic d
    D       = d*d';
    % Transformation into Voigt-scheme
    d_V     = [ D(1,1);
```

```
                D(2,2);
                D(3,3);
                sqrt(2)*D(2,3);
                sqrt(2)*D(1,3);
                sqrt(2)*D(1,2) ];
    % Calculation of the radius
    % Young's modulus
    E(j,i) = 1/(d_V'*(S*d_V));
    % Bulk modulus
    K(j,i) = 1/(3*U_V'*(S*d_V));
    end
end
%% Calculation of Poisson ratio and shear modulus
% Activate parallel processing
poolobj = parpool;
for i = 1:1:n
    for j = 1:1:m
    % Direction vector d with radius r=1
    d       = [ sin(phi(1,j))*cos(theta(1,i));
                sin(phi(1,j))*sin(theta(1,i));
                cos(phi(1,j)) ];
    % Transformation into tensor D, d dyadic d
    D       = d*d';
    % Transformation into Voigt-scheme
    d_V     = [ D(1,1);
                D(2,2);
                D(3,3);
                sqrt(2)*D(2,3);
                sqrt(2)*D(1,3);
                sqrt(2)*D(1,2) ];
    %
                for k = 1:1:o
                % Normal vector with radius r=1
                nn(1,k) = -cos(phi(1,j))*cos(theta(1,i))*cos(psi(1,k))
                    +...
                            sin(theta(1,i))*sin(psi(1,k));
                nn(2,k) = -cos(phi(1,j))*sin(theta(1,i))*cos(psi(1,k))
                    +...
                           -cos(theta(1,i))*sin(psi(1,k));
                nn(3,k) =  sin(phi(1,j))*cos(psi(1,k));
                        % Very small vector elements are set to exact
                           zero
                        for q = 1:1:3
                        if abs(nn(q,k)) <= 1e-6
                        nn(q,k) = 0;
                        else
                        end
                        end
                % Transformation of the normal vector into tensor N,
                % nn dyadic nn
                N   = nn(:,k)*nn(:,k)';
                % Transformation into Voigt-scheme
                n_V = [ N(1,1);
                        N(2,2);
                        N(3,3);
                        sqrt(2)*N(2,3);
                        sqrt(2)*N(1,3);
                        sqrt(2)*N(1,2) ];
                % Calculation of Tensor M
                M   = sqrt(2)/2*(d*nn(:,k)'+nn(:,k)*d');
                % Transformation into Voigt-scheme
                m_V = [ M(1,1);
                        M(2,2);
                        M(3,3);
                        sqrt(2)*M(2,3);
                        sqrt(2)*M(1,3);
                        sqrt(2)*M(1,2) ];
                % Calculation of Poisson ratio for every psi
                nu(1,k) = -E(j,i)*d_V'*(S*n_V);
```

```
                % Calculation of shear modulus for every psi
                G(1,k)   = 1/(2*m_V'*(S*m_V));
                end
    % Using of the criteria for Poisson ratio
    nu_max(j,i) = max(nu);
    nu_min(j,i) = min(nu);
    nu_avg(j,i) = sum(nu)/o;
    % Using of the criteria for shear modulus
    G_max(j,i)  = max(G);
    G_min(j,i)  = min(G);
    G_avg(j,i)  = sum(G)/o;
    end
end
% Deactivate parallel processing
delete(poolobj);
%% Transformation of spherical coordiantes into cartesian coordinates
for i = 1:1:n
    for j = 1:1:m
    % Young's modulus
    x_E(j,i)       = E(j,i)*sin(phi(1,j))*cos(theta(1,i));
    y_E(j,i)       = E(j,i)*sin(phi(1,j))*sin(theta(1,i));
    z_E(j,i)       = E(j,i)*cos(phi(1,j));
    % Bulk modulus
    x_K(j,i)       = K(j,i)*sin(phi(1,j))*cos(theta(1,i));
    y_K(j,i)       = K(j,i)*sin(phi(1,j))*sin(theta(1,i));
    z_K(j,i)       = K(j,i)*cos(phi(1,j));
    % Poisson ratio
    % 1. Maximum / 2. Minimum / 3. Average
    x_nu_max(j,i) = nu_max(j,i)*sin(phi(1,j))*cos(theta(1,i));
    y_nu_max(j,i) = nu_max(j,i)*sin(phi(1,j))*sin(theta(1,i));
    z_nu_max(j,i) = nu_max(j,i)*cos(phi(1,j));
    x_nu_min(j,i) = nu_min(j,i)*sin(phi(1,j))*cos(theta(1,i));
    y_nu_min(j,i) = nu_min(j,i)*sin(phi(1,j))*sin(theta(1,i));
    z_nu_min(j,i) = nu_min(j,i)*cos(phi(1,j));
    x_nu_avg(j,i) = nu_avg(j,i)*sin(phi(1,j))*cos(theta(1,i));
    y_nu_avg(j,i) = nu_avg(j,i)*sin(phi(1,j))*sin(theta(1,i));
    z_nu_avg(j,i) = nu_avg(j,i)*cos(phi(1,j));
    % Shear modulus
    % 1. Maximum / 2. Minimum / 3. Average
    x_G_max(j,i)  = G_max(j,i)*sin(phi(1,j))*cos(theta(1,i));
    y_G_max(j,i)  = G_max(j,i)*sin(phi(1,j))*sin(theta(1,i));
    z_G_max(j,i)  = G_max(j,i)*cos(phi(1,j));
    x_G_min(j,i)  = G_min(j,i)*sin(phi(1,j))*cos(theta(1,i));
    y_G_min(j,i)  = G_min(j,i)*sin(phi(1,j))*sin(theta(1,i));
    z_G_min(j,i)  = G_min(j,i)*cos(phi(1,j));
    x_G_avg(j,i)  = G_avg(j,i)*sin(phi(1,j))*cos(theta(1,i));
    y_G_avg(j,i)  = G_avg(j,i)*sin(phi(1,j))*sin(theta(1,i));
    z_G_avg(j,i)  = G_avg(j,i)*cos(phi(1,j));
    end
end
%% Plot of Young's modulus and Bulk modulus
% Colormap
map1 = [0.3, 0, 0
        0.4, 0, 0
        0.5, 0, 0
        0.6, 0, 0
        0.8, 0, 0
        1.0, 0, 0];
% Young's modulus
a = figure(1);
set(a, 'Units', 'centimeters', 'Position', [15, 10, 12, 10]);
% Plot of the surface in cartesian coordiantes. The fourth argument
% "E" respectively "K" is for the correct color.
hold on
surf(x_E, y_E, z_E, E,'FaceColor','interp','FaceAlpha',1.0,'LineWidth
    ',...
     0.01,'EdgeAlpha',0.2,'EdgeColor','w');
hold off
grid off
```

```
box off
set(gca,...
        'XTick',[],...
        'YTick',[],...
        'ZTick',[],...
        'XColor','w',...
        'YColor','w',...
        'ZColor','w');
colormap(map1);
colormap(flipud(colormap));
c = colorbar('eastoutside','Position',[0.87 0.27 .02 .5],'FontSize'
    ,10);
c.Label.String = '{\it{Y}} [GPa]';
c.Label.FontName = 'Times New Roman';
% Bulk modulus
b = figure(2);
set(b, 'Units', 'centimeters', 'Position', [15, 10, 12, 10]);
hold on
surf(x_K, y_K, z_K, K,'FaceAlpha',1.0,'EdgeAlpha',0.2,'LineWidth'
    ,....
     0.01,'EdgeColor','w');
hold off
grid off
box off
set(gca,...
        'XTick',[],...
        'YTick',[],...
        'ZTick',[],...
        'XColor','w',...
        'YColor','w',...
        'ZColor','w');
colormap(map1);
h = colorbar('eastoutside','Position',[0.8 0.3 .02 .4],'FontSize',10)
    ;
set(h,'YTickLabel',cellstr(num2str(reshape(get(h,'YTick'),[],1),'%0.2
    f')));
h.Label.String = '{\it{K}} [GPa]';
h.Label.FontName = 'Times New Roman';
%% Plot of Poisson ratio
f = figure(3);
set(f, 'Units', 'centimeters', 'Position', [15, 10, 10, 8]);
hold on
h1 = surf(x_nu_max, y_nu_max, z_nu_max, nu_max,'FaceColor','interp'
    ,...
          'FaceAlpha',1.0,'LineWidth',0.01,'EdgeAlpha',0.2,'EdgeColor
              ','w');
% h2 = surf(x_nu_min, y_nu_min, z_nu_min, nu_min,'FaceColor','interp
    ',...
%           'FaceAlpha',1.0,'LineWidth',0.01,'EdgeAlpha',0.2,'
    EdgeColor','w');
% h3 = surf(x_nu_avg, y_nu_avg, z_nu_avg, nu_avg,'FaceColor','interp
    ',...
%           'FaceAlpha',1.0,'LineWidth',0.01,'EdgeAlpha',0.2,'
    EdgeColor','w');
hold off
grid off
box off
set(gca,...
        'XTick',[],...
        'YTick',[],...
        'ZTick',[],...
        'XColor','w',...
        'YColor','w',...
        'ZColor','w');
colormap(map1);
g = colorbar('southoutside','Position',[0.32 0.27 .4 .02],'FontSize'
    ,10);
g.Label.String = '{\it{\nu}}_{max} [-]';
g.Label.FontName = 'Times New Roman';
```

```
%% Plot of shear modulus
t = figure(4);
set(t, 'Units', 'centimeters', 'Position', [15, 10, 10, 8]);
hold on

h4 = surf(x_G_max, y_G_max, z_G_max, G_max,'FaceColor','interp',...
          'FaceAlpha',1.0,'LineWidth',0.01,'EdgeAlpha',0.2,'EdgeColor
              ','w');
% h5 = surf(x_G_min, y_G_min, z_G_min, G_min,'FaceColor','interp',...
%           'FaceAlpha',1.0,'LineWidth',0.01,'EdgeAlpha',0.2,'
    EdgeColor','w');
% h6 = surf(x_G_avg, y_G_avg, z_G_avg, G_avg,'FaceColor','interp',...
%           'FaceAlpha',1.0,'LineWidth',0.01,'EdgeAlpha',0.2,'
    EdgeColor','w');
hold off
grid off
box off
set(gca,...
        'XTick',[],...
        'YTick',[],...
        'ZTick',[],...
        'XColor','w',...
        'YColor','w',...
        'ZColor','w');
colormap(map1);
d = colorbar('southoutside','Position',[0.33 0.20 .4 .02],'FontSize'
    ,10);
d.Label.String = '{\it{G}}_{max} [GPa]';
d.Label.FontName = 'Times New Roman';
```

References

1. Weng, Y., Dong, H., Dong, H., Gan, Y. (eds.): Advanced Steels. Springer, Berlin (2011). https://doi.org/10.1007/978-3-642-17665-4
2. Altenbach, H., Altenbach, J., Kissing, W.: Mechanics of Composite Structural Elements. Springer, Berlin (2004). https://doi.org/10.1007/978-3-662-08589-9
3. Langston, L.: Each blade a single crystal. Am. Sci. **103**(1), 30 (2015). https://doi.org/10.1511/2015.112.30
4. Altenbach, H.: Kontinuumsmechanik: Einführung in die materialunabhängigen und materialabhängigen Gleichungen, 3rd edn. Springer, Berlin (2015). https://doi.org/10.1007/978-3-662-47070-1
5. Lai, W., Rubin, D., Krempl, E.: Introduction to Continuum Mechanics, 4th edn. Butterworth-Heinemann, Oxford (2009)
6. Skrzypek, J.J., Ganczarski, A.W. (eds.): Mechanics of Anisotropic Materials. Springer, Berlin (2015). https://doi.org/10.1007/978-3-319-17160-9_1
7. Bertram, A.: Elasticity and Plasticity of Large Deformations: An Introduction, 3rd edn. Springer, Berlin (2012). https://doi.org/10.1007/978-3-642-24615-9
8. Nye, J.F.: Physical Properties of Crystals. Oxford University Press, Oxford (1985)
9. Voigt, W.: Lehrbuch der Kristallphysik (mit Ausschluss der Kristalloptik). Vieweg+Teubner Verlag, Berlin (1928). https://doi.org/10.1007/978-3-663-15884-4
10. Fedorov, F.I.: Theory of Elastic Waves in Crystals. Plenum Press, New York (1968). https://doi.org/10.1007/978-1-4757-1275-9
11. Cowin, S.C.: Properties of the anisotropic elasticity tensor. Quart. J. Mech. Appl. Math. **42**(2), 249–266 (1989). https://doi.org/10.1093/qjmam/42.2.249
12. Coleman, B.D., Noll, W.: Material symmetry and thermostatic inequalities in finite elastic deformations. Arch. Ration. Mech. Anal. **15**(2), 87–111 (1964). https://doi.org/10.1007/BF00249520
13. Ting, T.C.T.: Generalized Cowin–Mehrabadi theorems and a direct proof that the number of linear elastic symmetries is eight. Int. J. Solids Struct. **40**(25), 7129–7142 (2003). https://doi.org/10.1016/S0020-7683(03)00358-5
14. Xiao, H., Bruhns, O.T., Meyers, A.: Existence and uniqueness of the integrable-exactly hypoelastic equation $\overset{\circ}{\boldsymbol{\tau}}{}^{\star} = \lambda(\mathrm{tr}\boldsymbol{D})\boldsymbol{I} + 2\mu\boldsymbol{D}$ and its significance to finite inelasticity. Acta Mech. **138**(1), 31–50 (1999). https://doi.org/10.1007/BF01179540
15. Weyl, H.: The Classical Groups: Their Invariants and Representations, 2nd edn. Princeton University Press, Princeton (1997). 15. print and 1. paperback print
16. Ting, T.C.T.: Anisotropic Elasticity: Theory and Applications. Oxford University Press, Oxford (1996)
17. Lurie, A.I.: Theory of Elasticity. Springer, Berlin (2005). https://doi.org/10.1007/978-3-540-26455-2
18. Böhlke, T., Brüggemann, C.: Graphical representation of the generalized Hooke's law, Technische Mechanik 21(2):145–158 (2001). http://www.uni-magdeburg.de/ifme/zeitschrift_tm/2001_Heft2/Boehlke_Brueggeman.pdf. Accessed 7 Dec 2017
19. Rychlewski, J.: Unconventional approach to linear elasticity. Arch. Mech. **47**(2), 149–171 (1995)
20. He, Q.-C., Curnier, A.: A more fundamental approach to damaged elastic stress–strain relations. Int. J. Solids Struct. **32**(10), 1433–1457 (1995). https://doi.org/10.1016/0020-7683(94)00183-W

21. Reuss, A.: Berechnung der Fliegrenze von Mischkristallen auf Grund der Plastizitätsbedingung für Einkristalle. J. Appl. Math. Mech. **9**(1), 49–58 (1929). https://doi.org/10.1002/zamm.19290090104
22. Hill, R.: The elastic behaviour of a crystalline aggregate. Proc. Phys. Soc. Sect. A **65**(5), 349 (1952). https://doi.org/10.1088/0370-1298/65/5/307
23. Mehrabadi, M.M., Cowin, S.C.: Eigentensors of linear anisotropic elastic materials. Quart. J. Mech. Appl. Math. **43**(1), 15–41 (1990). https://doi.org/10.1093/qjmam/43.1.15
24. Mandel, J.: Eigentensors of linear anisotropic elastic materials. Quart. J. Mech. Appl. Math. **1**, 3–30 (1962)
25. Thomson, W.: Mathematical theory of elasticity: elasticity. Encycl. Br. **7**, 819–825 (1878)
26. Sutcliffe, S.: Spectral decomposition of the elasticity tensor. J. Appl. Mech. **59**(4), 762–773 (1992)
27. Golub, G.H., Loan, C.F.V.: Matrix Computations (Johns Hopkins Studies in Mathematical Sciences), 3rd edn. Johns Hopkins University Press, Baltimore (1996)
28. Marmier, A., Lethbridge, Z.A., Walton, R.I., Smith, C.W., Parker, S.C., Evans, K.E.: ElAM: a computer program for the analysis and representation of anisotropic elastic properties. Comput. Phys. Commun. **181**(12), 2102–2115 (2010). https://doi.org/10.1016/j.cpc.2010.08.033
29. Gaillac, R., Pullumbi, P., Coudert, F.-X.: ELATE: an open-source online application for analysis and visualization of elastic tensors. J. Phys. Condens. Matter **28**(27), 275201 (2016). https://doi.org/10.1088/0953-8984/28/27/275201
30. dell'Isola, F., Sciarra, G., Vidoli, S.: Generalized Hooke's law for isotropic second gradient materials. Proc. R. Soc. A Math. Phys. Eng. Sci. **465**(2107), 2177–2196 (2009). https://doi.org/10.1098/rspa.2008.0530
31. Auffray, N., Quang, H.L., He, Q.: Matrix representations for 3D strain-gradient elasticity. J. Mech. Phys. Solids **61**(5), 1202–1223 (2013). https://doi.org/10.1016/j.jmps.2013.01.003
32. Aßmus, M., Nordmann, J., Naumenko, K., Altenbach, H.: A homogeneous substitute material for the core layer of photovoltaic composite structures. Compos. Part B Eng. **112**, 353–372 (2017). https://doi.org/10.1016/j.compositesb.2016.12.042